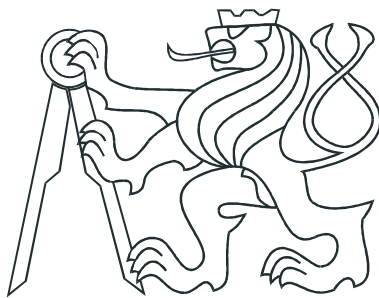


České vysoké učení technické v Praze
Fakulta jaderná a fyzikálně inženýrská



Výzkumný úkol

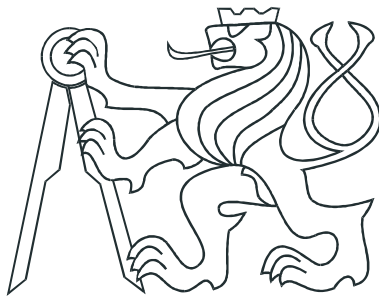
....název.....

Praha, 2009

Autor: Olga Hájková

Vedoucí práce: Mgr. Jaroslav Bielčík, Ph.D.

Czech Technical University in Prague
Faculty of Nuclear Sciences and Physical
Engineering



Research

.....title..

Prague, 2009

Author: Olga Hájková

Supervisor: Mgr. Jaroslav Bielčík, Ph.D.

Introduction

Quarks and leptons are fundamental constituents of matter (Fig.1). Quarks are constituents of hadrons: mesons and baryons. There are six different flavors of quarks: up, down, strange, charm, beauty and top. Quarks can exist only inside hadrons because they are confined there. Beside the other quantum numbers quarks carry also a color charge that is associated with the strong interaction.

Similarly to quarks, there are six types of leptons: electrons, muons, taus, and corresponding neutrinos. The electron, the muon, and the tau carry a negative charge, whereas the three neutrinos carry no charge. Charged leptons interact via electromagnetic and weak forces, while for neutral leptons only the weak interaction has been observed.

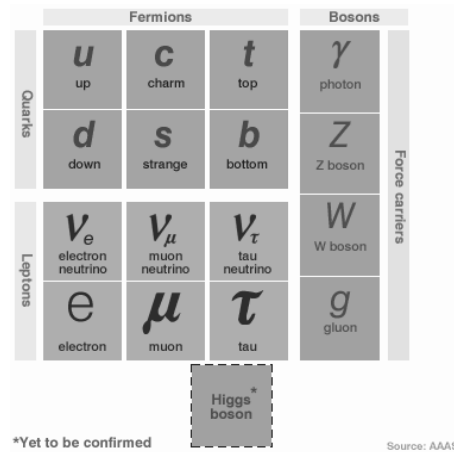


Figure 1: Fundamental particles of a Standard model. Each particle has also its antiparticle.

The third group of elementary particles are interaction carrier particles: gluons, W^\pm mesons, Z^0 mesons and photons.

The individual category is the Higgs boson that is assumed to be responsible for particle properties associated with mass. The Higgs boson has not yet been observed. Every particle in Fig. 1 has its antiparticle.

The objective of the high energy physics is the detection and measurement of the properties and behavior of these fundamental particles, along with the understanding of the forces acting among them. These four forces are: the electromagnetic force, the strong force, the weak force, and gravitation.

This work is about heavy ion physics. In heavy ion physics by the means of nucleus-nucleus collisions, the properties of the hot and dense nuclear matter is investigated.

Contents

| | | |
|----------|---|-----------|
| 1 | Heavy ion physics | 6 |
| 1.1 | QGP and its signatures | 6 |
| 1.2 | Collision geometry and centrality | 7 |
| 1.3 | Space-time evolution of matter | 8 |
| 2 | Charmonium system and production mechanism | 10 |
| 2.1 | J/ψ discovery | 10 |
| 2.2 | Charmonia family | 10 |
| 2.3 | Theoretical model of charmonia production | 11 |
| 2.4 | Different channels of J/ψ production | 13 |
| 2.5 | J/ψ production in hadron-hadron collisions | 13 |
| 3 | Experimental setup | 16 |
| 3.1 | The Relativistic Heavy Ion Collider | 16 |
| 3.2 | STAR | 17 |
| 4 | J/ψ analysis in d+Au collisions at $\sqrt{s} = 200\text{GeV}$ at the STAR | 20 |
| 4.1 | The track selection | 21 |
| 4.2 | Electron identification | 23 |
| 4.3 | The raw J/ψ spectrum | 25 |
| 5 | Acceptance and efficiency | 27 |
| 5.1 | J/ψ reconstruction efficiency | 27 |
| 5.2 | Electron identification efficiency | 30 |
| 6 | Corrected J/ψ pT spectrum | 33 |

1 Heavy ion physics

1.1 QGP and its signatures

Quantum Chromodynamics (QCD) is a theory of strong interaction between quarks and gluons. Quarks have a quantum number called color and they are confined by gluons in colorless hadrons. There are three possible colors of quarks: red, blue and green, and three possible anticolors of antiquarks. The interaction between two coloured particles is characterized by the strong interaction coupling constant α_s :

$$\alpha_s = \frac{12\pi}{(33 - 2N_f)\ln(\frac{Q^2}{\lambda_{QCD}})}, \quad (1)$$

where Q^2 is four momentum transfer, N_f is the number of quark flavours and λ_{QCD} is the typical QCD scale ($\lambda_{QCD} \approx 0.2\text{GeV}$). The coupling constant α_s for the strong force becomes smaller at shorter distances. This effect is known as asymptotic freedom. Another important effect is the color confinement. The confinement means that the force between quarks is stronger at larger distances and quarks seem to remain confined at small distances. The coupling constant α_s decreases with an increase in momentum transfer and decreases in the environment of high temperature and/or densities too. When the system reaches the critical temperature, the color confinement is broken and matter passes through phase transition from the confined nuclear matter to the deconfined state. This is predicted from calculations on lattice QCD. A phase diagram of hadronic matter shown in Fig. 2 as a function of temperature and the baryon density. The assumed phase transition line between hadron gas and quark gluon plasma (QGP) is denoted.

Quark gluon plasma is a new state of matter which is composed of deconfined quarks and gluons. QGP is believed to exist in the early universe, about 10^{-6} second after the Big Bang. High energy heavy ion collisions provide a possibility to produce QGP in the laboratory. Current calculations show that the transition happens around the critical temperature $T_c = 150 - 180\text{MeV}$, which corresponds to an energy density of about $0.3 - 1.0\text{GeV}/\text{fm}^3$ [1].

Even if QGP is produced in a laboratory, its identification is difficult because of its very short lifetime. Its impossible to directly observe its thermodynamics variables. So, its necessary to rely on indirect measurements of QGP formation. Certain signatures of the phase transition could allow us to establish whether the matter is deconfined or not. Observable signatures in high energy heavy ion collisions could be divided into three classes: hard, electromagnetic and soft probes. Hard probes that included J/ψ suppression are of the most interest of this work.

As mentioned above also the J/ψ suppression research has been considered as one of the most promising signatures for QGP formation since Matsui and Satz proposed it [3]. Due to color screening of the surrounding nuclear matter a J/ψ are expected to disassociate under certain conditions. Therefore, J/ψ has been used as a tool of searching for QGP formation in heavy ion collisions.

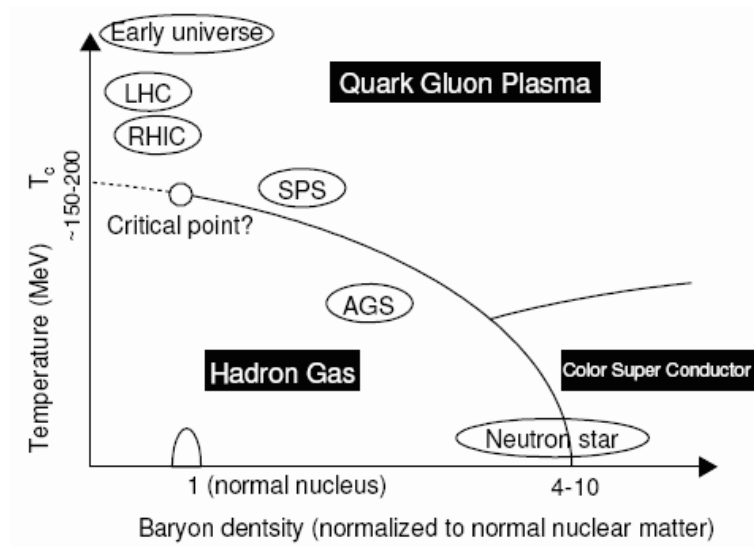


Figure 2: A phase diagram of matter. Assumed phase transition lines are denoted[2].

1.2 Collision geometry and centrality

Geometry of two colliding nuclei is very important for collision dynamics. As illustrated in Fig.3, the nucleons in collision can be classified into two groups, spectators and participants. The nucleons in the overlap region participate on the collision, so they are called participants. The nucleons in the other nucleus region are called spectators.

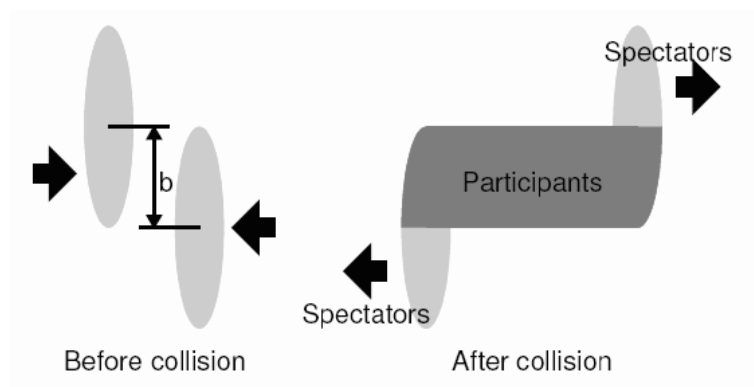


Figure 3: Spectators and participants - active and passive regions of colliding nuclei [2].

The main parameter of colliding nuclei is the impact parameter b . The impact parameter denotes the sizes of spectator and participant groups. This way, we can speak about central and peripheral collisions. If the impact parameter b is nearly zero or very small, almost all nucleons participate in the collision, and the collision is called central. When the impact parameter is large, the collision is called peripheral. The central and peripheral collisions are shown in Fig.4.

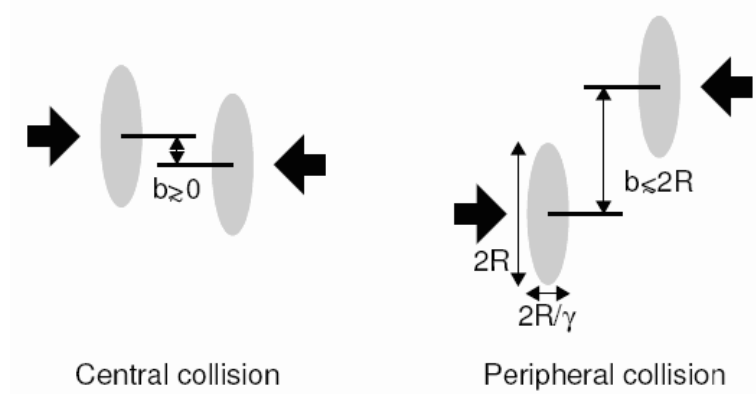


Figure 4: A central collision with a small impact parameter on the left and a peripheral collision with a large impact parameter on the right [2].

The binary collision is an interaction between two free particles, in terms of heavy ion collisions it is an interaction between two nucleons. The nuclear modification factor R_{AA}

We define the nuclear modification factor as R_{AA} is what we get divided by what we expect. By definition, processes that scale with the number of underlying nucleon-nucleon collisions (aka N_{binary}) will produce $R_{AA}=1$.

The nuclear modification factor R_{AA} is the number calculated from measured value divided by expected value. Processes that scale with the number of underlying nucleon-nucleon collisions will produce $R_{AA}=1$.

R_{AA} quantifies the effect of A+A compared to p+p collisions on particular particle yields for point/like processes

It is defined as the ratio of the particle yield in A+A collision to the yield in a p+p collision scaled by the mean number of binary collisions in the A+A sample.

1.3 Space-time evolution of matter

The evolution of matter created in high-energy heavy ion collisions can be illustrated by the space-time diagram (Fig.5), with the longitudinal coordinate z and transversal coordinate t . It may be viewed as evolving through the following stages that are expected to exist from the initial collision to the final hadronic phase: It is assumed that the space-time evolution depends only on the proper

time $\tau = \sqrt{t^2 - z^2}$:

1) At the proper time $\tau = 0$ a huge amount of energy is disengaged in a tiny volume. The expected energy density is high enough to form the deconfined matter of quarks and gluons. Matter in this stage is not in the thermal equilibrium. The dynamics in this phase could be described by a cascade of colliding partons.

2) Deconfined state of partons in thermal equilibrium. This phase is called the QGP stage. The QGP then evolves like fluid, expands and cools down with according to hydrodynamic laws.

3) At $\tau = \tau_c$ the system has reached the critical temperature T_c and starts to hadronize. If the transition is first order, matter passes through the mixed phase consisting of gluons, quarks and hadrons.

4) The hadronization of the system is finishing and hadrons are interacting with each other till the temperature drops to the freeze-out temperature.

5) At the freeze-out temperature hadrons finish interacting and leave the collision region.

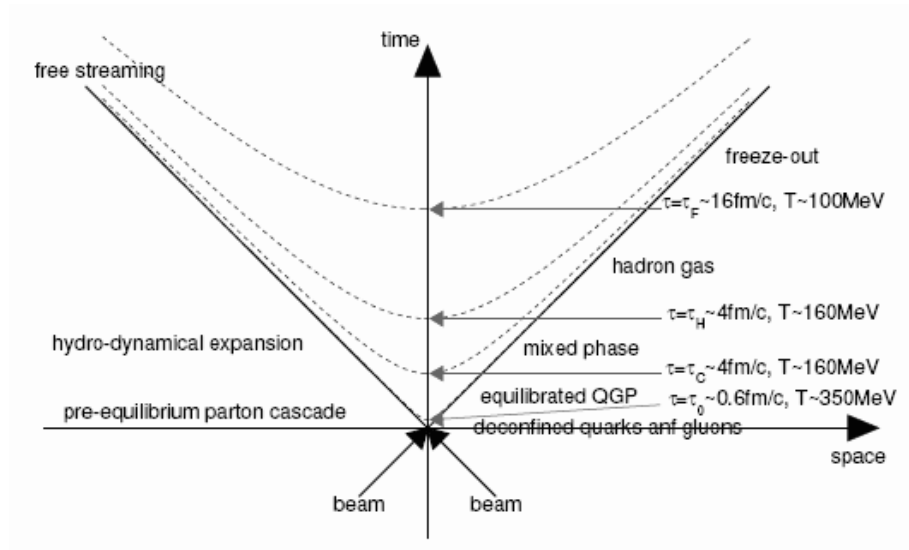


Figure 5: Time space evolution of matter created in high energy heavy ion collisions [2].

2 Charmonium system and production mechanism

2.1 J/ψ discovery

The J/ψ meson was discovered in 1974 in two independent laboratories simultaneously. At Stanford at SPEAR collider in e^+e^- annihilation, by Burton Richter and at Brookhaven National Laboratory at the alternating gradient synchrotron (AGS) in p+Be collisions, by Samuel Ting. This new particle decayed slowly and did not fit into the framework of up, down, and strange quarks. The J/ψ discovery was the first firm experimental evidence for the fourth quark. Richter and Ting shared the Nobel Prize for their discovery in 1976.

2.2 Charmonia family

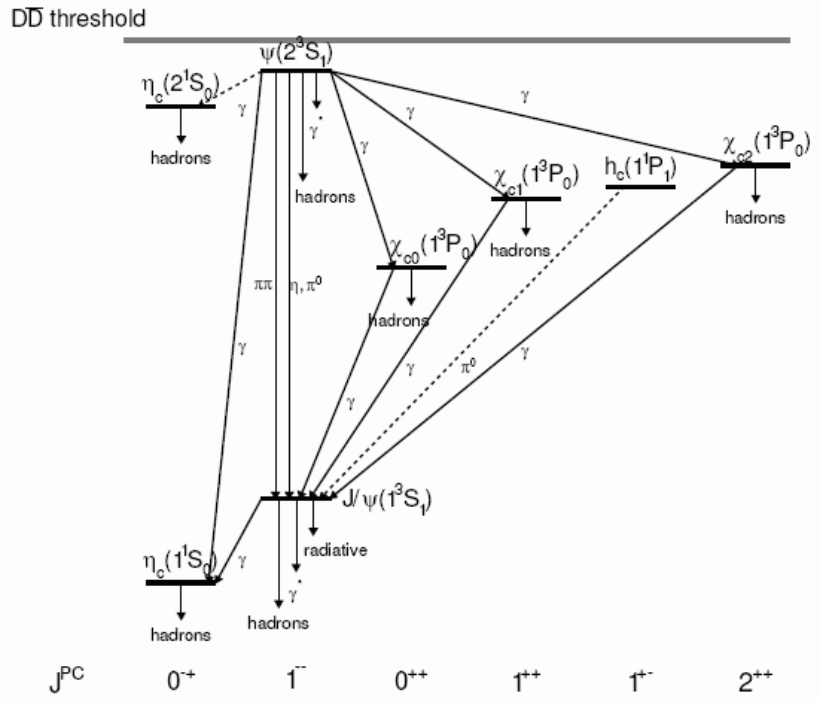


Figure 6: Charmonium model, the current state of knowledge of the charmonium system. The dashed line denotes uncertain transitions [2].

Quarkonium is a bound state of a heavy quark and antiquark pair. Quarkonium composed of a charm quark and antiquark pair is called charmonium, and quarkonium composed of a bottom quark-antiquark pair is called bottomonium. The schema of charmonium current state knowledge is illustrated in

Fig.6. Charmonium states can be classified by their principal quantum number n . This schema shows charmonia in the ground state ($n=1$) the J/ψ meson and ψ_c , and charmonia in the excited state ($n=2$) the ψ' meson and three states of χ_c . Excited state of charmonia could feed-down to J/ψ with emission of the photon. Feed-down means a decay into the J/ψ meson and photon.

J/ψ seem to be the most famous charmonium. Properties of the J/ψ meson and the other charmonium bound states are shown in Table??.

2.3 Theoretical model of charmonia production

Production of J/ψ from initial partons is divided into two steps. The first step is a $c\bar{c}$ pair production in hard scattering of the initial partons and the second one is hadronization into J/ψ from the $c\bar{c}$ pair. A more complicated part is obtaining the bound state from a $q\bar{q}$ pair (step 2), especially if the bound state is to be produced with the right angular momentum and spin quantum numbers. There are several theoretical models employed for quarkonium production: the color singlet model (CSM), the color evaporation model (CEM), the color octet model (COM). However, no of these models succeeded to make universal description of the quarkonium production. These models are briefly explained in the following section.

a) Color singlet model

The CSM was first proposed shortly after J/ψ discovery. It requires the colorless $c\bar{c}$ pair to be created with the same quantum numbers as the J/ψ meson. Fig.7 shows an example of the lowest order diagram of J/ψ production in the CSM, where the $c\bar{c}$ pair has 3S_1 and should be colorless as the J/ψ .

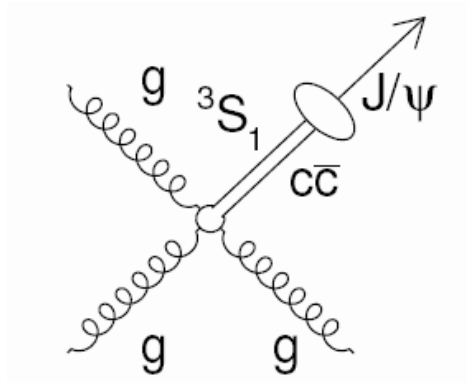


Figure 7: An example of the lowest order diagram for direct a J/ψ production from gluon (g) fusion with the color singlet model. The $c\bar{c}$ pair is in the color singlet state[1].

To conserve C parity, hard gluon emission is necessary in the color singlet

model. This model can describe the J/ψ production cross section in the photo-production, but failed to explain the p_T differential cross section in $p+\bar{p}$ collisions at the Tevatron at the FNAL [4].

b) Color evaporation model

The CEP was first proposed in 1977. In the CEM model the quarkonium production is processed in the same way as open heavy quark production with the restriction that the $c\bar{c}$ mass must be below the $D\bar{D}$ threshold [5]. The CEM does not have any constraints on color or other quantum numbers for the $c\bar{c}$ pair. The CEM assumes that the $c\bar{c}$ pair neutralizes its color by an interaction with collision-induced color field, called 'color evaporation'. In the CEM the J/ψ is formed through multiple soft gluon emissions that destroy the information on quantum numbers of the $c\bar{c}$ pair as shown in Fig.8.

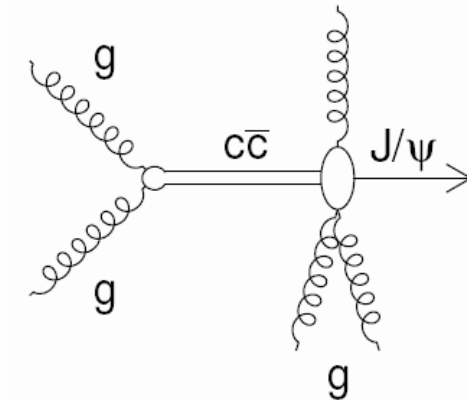


Figure 8: An example of the lowest order diagram for the direct J/ψ production from a gluon fusion with the color evaporation model [1].

The CEM describes a total hadro-production and photo-production of J/ψ at lower energies. The CEM predicts zero polarization of the J/ψ meson that is consistent in the lower p_T region, but that is not consistent in the intermediate and high p_T regions[1].

c) Color octet model

The color octet model (COM) was developed in the 1990's based on the non-relativistic QCD (NRQCD) framework[5]. The COM allows a J/ψ formation from a color octet $c\bar{c}$ pair with one or few soft gluons emissions. An example of the COM is shown in Fig.9. The COM has successfully reproduced the p_T distribution in $p + \bar{p}$ collisions and the total cross section at lower-energy experiments[1]. On the other hand, the COM predicts large transverse polarization, while large longitudinal polarization is observed experimentally.

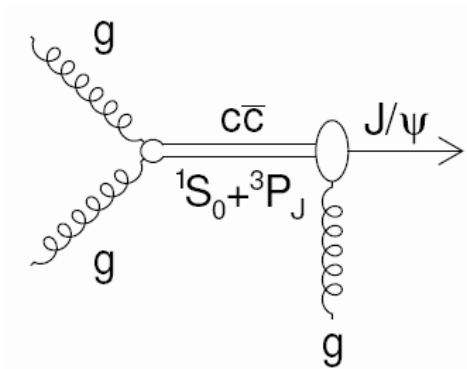


Figure 9: An example of the lowest order diagram for the direct J/ψ production from the gluon fusion with the COM [1].

2.4 Different channels of J/ψ production

J/ψ mesons actually measured in hadron-hadron collisions can have four different origins: a direct production of J/ψ , feed down from three χ_c states, feed down from a ψ' state, and a production from the decay of a bottom quark.

The part of measured J/ψ s from three χ_c states decays is represented by the ratio R_{χ_c} , and J/ψ s produced from the ψ' state are represented by the ratio $R_{\psi'}$ defined as follows:

$$R_{\chi_c} = \frac{1}{\sigma_{J/\psi}} \sum_{i=0}^2 BR(\chi_{ci} \rightarrow J/\psi + \gamma) \sigma_{\chi_{ci}} \quad (2)$$

$$R_{\psi'} = \frac{\sigma_{\psi'}}{\sigma_{J/\psi}} BR(\psi' \rightarrow J/\psi + X), \quad (3)$$

where $\sigma_{J/\psi}$ is a J/ψ cross section, $BR(\chi_c \rightarrow J/\psi + \gamma)$ is a branching ratio of the $\chi_c \rightarrow J/\psi$ decay, and $BR(\psi' \rightarrow J/\psi + X)$ is a branching ratio of the $\psi' \rightarrow J/\psi$ decay. The average value of R_{χ_c} is about 0.3, and $R_{\psi'}$ is assumed to be less than 0.1 [2]. Finally, the fraction of the J/ψ production from a bottom quark decay is represented by the ratio R_b and is about 0.014 [2]. To sum it up, the contributions to the J/ψ production from the 4 origins are:

1. Directly produced J/ψ s are about 0.6
2. J/ψ s produced from three χ_c states decay are about 0.3
3. J/ψ s produced from the ψ' decay are about 0.1
4. J/ψ s produced from the bottom quark decay are about 0.01

2.5 J/ψ production in hadron-hadron collisions

Since charm quarks are heavy, the production of charm quarks takes place only at the beginning of the collision. J/ψ may be formed before QGP formation.

On that account, medium effect on the J/ψ production can be categorized into two groups: cold nuclear matter effects and final state effects.

Cold nuclear matter effects take place before the QGP formation. The possible contribution to the modification of the J/ψ production are gluon shadowing and nuclear absorption.

Final state effects take place after the QGP formation. There are following contributions to the modification of the J/ψ production: color screening in QGP, recombination of J/ψ s from uncorrelated $c\bar{c}$ pairs, and the J/ψ interaction with secondary comoving hadrons. The final state effects are briefly described in the following section.

Color screening

The potential of a $q\bar{q}$ pair in vacuum can be described as follows:

$$V(r, T = 0) = -\frac{4}{3} \frac{\alpha_s(r)}{r} + \sigma r, \quad (4)$$

where r is the distance between quark and antiquark, σ is the string tension coefficient, and q is a color charge. In finite temperatures this potential is modified due to color screening:

$$V(r, T) = -\frac{\alpha_{eff}}{r} \exp\left(-\frac{r}{\lambda_D(T)}\right) + \sigma \lambda_D(T) \left[1 - \exp\left(-\frac{r}{\lambda_D(T)}\right)\right], \quad (5)$$

where $\lambda_D(T)$ is the Debye screening length. The Debye screening length depends on the temperature and decreases with its increase. It can be evaluated as follows:

$$\lambda_D(T) = \frac{1}{\sqrt{\left(\frac{N_c}{3} \frac{N_f}{6}\right) g^2 T}}, \quad (6)$$

where N_c is the degree of color freedom, N_f is the number of quark flavors, $g^2 = 4\pi\alpha_{eff}$, and T is the matter temperature. When the Debye screening length is smaller than the charmonium radius, quark and antiquark cannot stay longer in the bound state. For the QGP ($N_c = 3$, $N_f = 3$, $T = 200MeV$), the screening length is $\lambda_D = 0.33$ fm [4]. Since the J/ψ radius is 0.453fm, it predicates that $c\bar{c}$ pairs cannot stay in the bound state in the QGP at the temperature $T = 200MeV$.

J/ψ recombination

J/ψ production could be enhanced due to uncorrelated $c\bar{c}$ pairs recombination. This scenario is predicted at RHIC energies, and it is derived from the assumption that the number of recombined charmonia are approximately proportional to N_c^2/N_h , where N_c is the number of created charm quarks, and N_h is the number of produced hadrons. The charm production N_c increases faster

with \sqrt{s} , and scales with the number of inelastic nucleon-nucleon collisions, while N_h scales with the number of participant nucleons. Since the number of nucleon-nucleon collisions is sufficiently higher in more central collisions than the number of participant nucleons at RHIC energy, N_c^2/N_h leads to a higher value at a higher collision energy and in more central collisions. Hence, this effect cannot be negligible at the RHIC energy.

Comover interactions

An additional absorption of J/ψ by secondary hadrons called comovers occurs in the hadronic phase. The survival probability of J/ψ can be expressed as follows:

$$S_{co} = \exp\left(-\int d\tau \rho_{co}(\tau) \sigma_{co} v\right) \quad (7)$$

where τ is time, ρ_{co} is the comovers density, v is the relative velocity between the J/ψ and a secondary hadron, and σ_{co} is a cross section of the J/ψ absorption by comovers [5].

3 Experimental setup

3.1 The Relativistic Heavy Ion Collider

The Relativistic Heavy Ion Collider (RHIC) is located at the Brookhaven National Laboratory in Upton, New York. The RHIC started its operation in 2000. The whole RHIC complex is illustrated in Fig.10. Research at the RHIC is focuses on the study of a quark gluon plasma, the primordial state of matter that existed in the early universe. Key features of the nuclear environment at RHIC are a large number of produced particles and high momentum particles from hard parton-parton scattering. The goal is to obtain a fundamental understanding of the microscopic structure of these hadronic interactions at high energy densities[6].

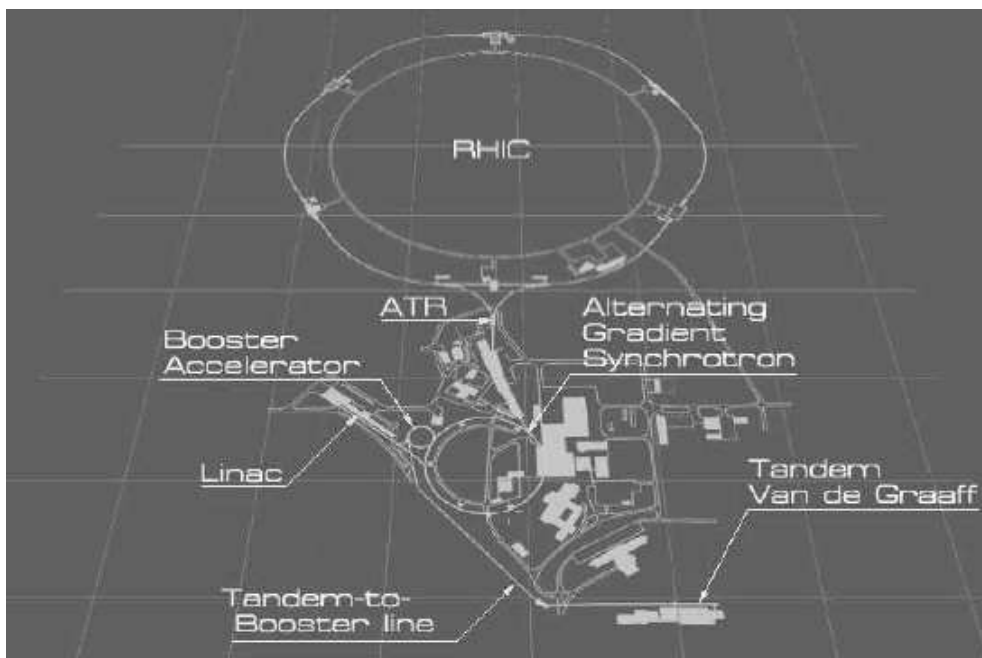


Figure 10: A schematic view of the RHIC complex [7].

The RHIC is an intersection storage ring (ISR) particle accelerator composed of two independent rings. Its designed to collide light nuclei as protons and heavy nuclei like Au, Cu as well. It is able to work out asymmetric collisions as $d+Au$ are. These collisions are important to study cold nuclear matter effects and distinguish them from hot nuclear matter effects. The RHIC has a circumference of 3834 m and 6 intersection points where particles collide. Originally there were 4 experiments at intersection points: STAR, PHENIX, BRAHMS

and PHOBOS. BRAHMS and PHOBOS completed their program already. The maximum center of mass energy per nucleon-nucleon pair for Au+Au collisions is $s_N N = 200$ GeV. It can also collide p+p up to 500 GeV and d+Au, Cu+Cu up to 200 GeV. In this analysis are presented data taken by the STAR detector. Before reaching the RHIC storage ring, each particle passes through several stages illustrated in Fig.9. Heavy ions started their acceleration in the Tandem Van de Graaf where ions are accelerated to an energy about 1 MeV per nucleon. Then ions are stripped of electrons and passed through the Tandem-to-Booster line, the Booster synchrotron. After the Booster ions have an energy about 95 MeV per nucleon. Next step is the Alternating Gradient Synchrotron (AGS) that was used for fixed target experiments in the past and where ions are accelerated to an energy of 8.86 GeV per nucleon. And finally ions are sent through the AGS-To-RHIC (ATR) transfer line. At the end of this process, ion bunches are sent by switching magnets to the one of two beam lines. Finally, the bunches are colliding into one of four interaction point.

3.2 STAR

The Solenoidal Tracker at the RHIC (STAR) is a massive detector that was designed especially for a study of the hadron production and search for signatures of the quark gluon plasma formation and its properties and for study of other physics effects which occur in the extreme conditions of a relativistic heavy-ion collision. Compared with other experiments at RHIC, it is unique in its full azimuthal coverage that making possible study of azimuthal particle correlations. Due to this and good coverage of pseudorapidity $\eta < 1.8$ the STAR detector is able to measure a wide variety of physics phenomena [6]. Most constituents of the STAR experiment are inside of a solenoidal magnet with an approximately uniform magnetic field ($B=0.5$ T maximally) parallel to the beam pipe. The most central tracking detector is the Time Projection Chamber (TPC) that is detailed discussed in the next subsection so as Barrel Electromagnetic Calorimeter (BEMC) data from that are used in this analysis. The general STAR detector schema is shown in Fig.11.

Time Projection Chamber (TPC)

The TPC (illustrated in Fig.12) is a central element located in the solenoidal magnet and having 4.2 m along the beam axis and 4 m in diameter. The TPC is a primary tracking device of the STAR detector and registers tracks of particles, measures their momentum, and identifies particles via the ionization loss (dE/dx). Its acceptance covers 1.8 units of pseudorapidity through the full azimuthal angle. Charged particles with momenta greater than 100 MeV/c are recorded. More than 3000 tracks per event are routinely reconstructed [9].

The TPC is an empty volume filled with an argon+diomethan gas mixture (10 percent of methane, 90 percent of argon), in a well defined, uniform, electric field of 135 V/cm. This gas was chosen with respect to its minimum attenuation of the drifting electrons. The trajectories of primary ionizing particles are recon-

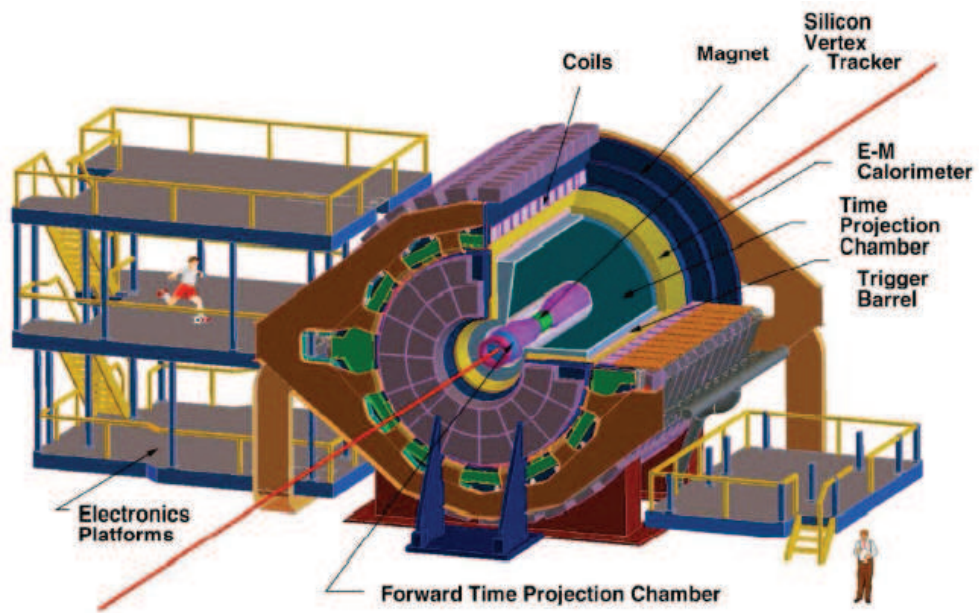


Figure 11: The experimental setup of the STAR detector [8].

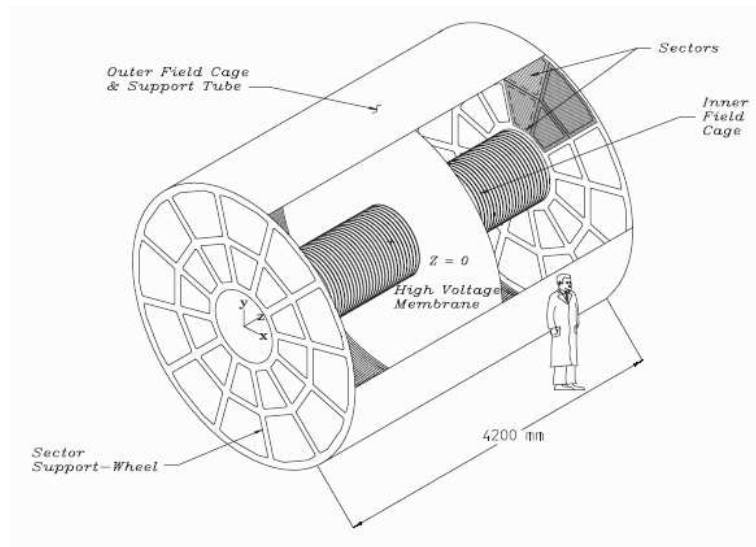


Figure 12: STAR TPC schema [9].

structured from released secondary electrons drifting to the readout end caps at the ends of the chamber. Limits of the TPC particle identification are diffusion

of the drifting electrons and their limit number necessary for the definition of the position, ionization energy loss fluctuations and finite track length. The uniform electric field required to drift the electrons is defined by a thin conductive membrane at the center of the TPC that is operated at 28kV. The endcaps are at ground. The space between the central membrane and the anode planes is divided into 182 equally segments. These dividing rings are biased by chain of 2M resistors which provide a uniform gradient between the central membrane and the grounded endcaps[9] The readout endcap modules are split into 12 sectors around the beampipe. Each sector is divided into outer and inner sectors in the readout plane. In the inner sector the density of tracks is bigger so the pads are smaller than in the outer sector. The tracks (x,y coordinates) are reconstructed from the pad signals and from the electron drift time (z coordinate). The dE/dx is calculated from the energy loss measured on up to 45 pad rows. Ionization energy loss dE/dx is the powerful device used to identify particles. The energy loss per unit length is described by the Bethe-Bloch formula[10].

The Barrel Electromagnetic Calorimeter (BEMC)

The BEMC is located inside of the STAR solenoid and covers $|\eta| < 1$ and full azimuthal angle, thus matching the acceptance for full TPC tracking. The Barrel electromagnetic calorimeter (BEMC) is included of 120 calorimeter modules, each of them is segmented into 40 towers. Every tower is oriented in the direction of the interaction point. The inner surface of the BEMC has a radius of about 220cm and the outer radius is about 250 cm. In each module there are 21 active plastic and lead scintillating layers. The calorimeter has a total depth of approximately twenty radiation lengths[11]. The BEMC provides large acceptance for photons, electrons and π^0 mesons. All these measurements require precise electromagnetic shower reconstruction with high spatial resolution. The EMC tower energy that was used in this analysis provides a high resolution, linear measure of the full energy of electrons that strike it. Hadrons typically deposit far less than their total energy in a tower. Due to this fact, E/p is a powerful electron identification tool.

4 J/ψ analysis in d+Au collisions at $\sqrt{s} = 200\text{GeV}$ at the STAR

In this work an update analysis of J/ψ meson production in d+Au collisions at $\sqrt{s} = 200\text{GeV}$ using data taken during the 2008 run with the STAR experiment at BNL is presented. Events used for this analysis were that with the Z axis component of the primary vertex from -30 cm to 30 cm from the detector mid-point and taken with a minimum bias trigger. The total number of Minimum Bias events and the number of events pass through event cuts are listed in Tab.1.

| | |
|-----------------------------|-------|
| <i>MinBiasdata</i> | 46M |
| <i>zVertexcut</i> | 32.5M |
| <i>N_{BEMC} cut</i> | 31M |

Table 1: The total number of events before any cuts and after events cuts.

Another criteria required in this analysis is $N_{BEMC} \geq 1$, the number of tracks matched to the BEMC. Next event criterium used in this analysis is a pseudo-rapidity cut. Daughter electron or positron which pseudo-rapidity η is in the absolute value larger then 1 cannot be reconstructed in the TPC. So only positrons and electrons with the pseudo-rapidity in this range were accepted. The pseudo-rapidity distribution is shown in Fig.13. All of event cuts used in this analysis are listed in Tab.2.

| | |
|-------------|-----------------|
| $ zVertex $ | $< 30\text{cm}$ |
| N_{BEMC} | ≥ 1 |
| $ \eta $ | $< 1\text{cm}$ |

Table 2: The summary of event cuts used in this analysis.

The reference multiplicity is a characteristic quantity defined as a number of charged particles at mid-rapidity $|\eta| < 0.5$. The reference multiplicity is related to the event centrality through the Glauber model. The Glauber model describes nuclear collision as an ensemble of nucleon-nucleon collisions in the overlap region in a plane transversal to the beam line[23]. In this analysis collisions have been distributed into three centrality classes, 0-20, 20-40 and 40-100 percent of the most central collisions. The multiplicity distribution is shown in Fig.14.

The mean of participants and the number of binary collisions for each centrality class are listed in Tab.3.

This chapter is contains of two principal parts. Firstly the tracks selection is discussed and than the electron identification is presented. These steps was done for all centrality together.

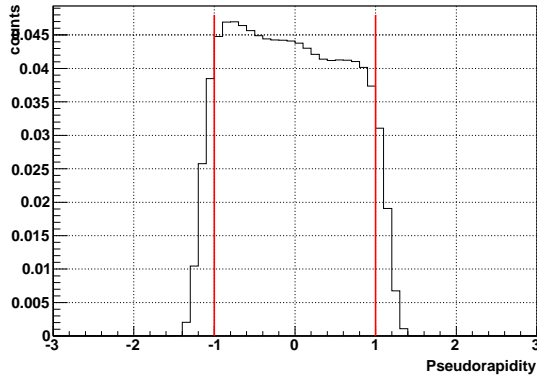


Figure 13: The pseudo-rapidity distribution. Red lines denote used cut ($|\eta| < 1$).

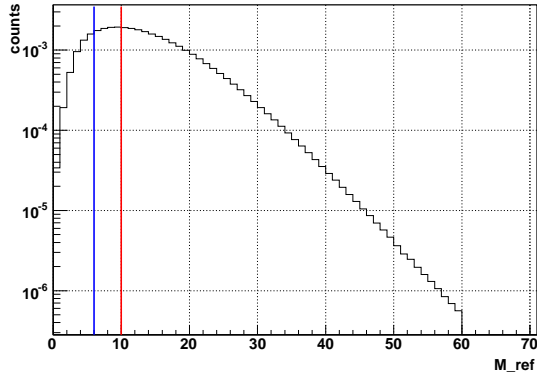


Figure 14: The multiplicity distribution. Blue and red lines divided centrality classes.

4.1 The track selection

Particle tracks were reconstructed from registered hits in the TPC readout system. The number of these fit points is the main criterium for a track quality selection. Track with only few hits could be randomly associated hits. Tracks reconstructed from more than 19 points were accepted ($N_{fit} \geq 20$). For an elimination of double counting, another cut was used, the number of fit points over the number of maximum fit points $N_{fitmax} > 0.51$. Both fit points cuts are illustrated in Fig.15 and Fig.16.

In order to eliminate a contamination from secondary electron tracks, the global DCA cut ($gDCA < 2.0cm$) was used. The gDCA is a distance of a track to the global vertex of the event.

The J/ψ meson has a large mass, therefore the produced electrons and

| Centrality class | Multiplicity | $N_{participants}$ | $N_{collisions}$ |
|------------------|-----------------------|--------------------|------------------|
| 0 – 20 | $M_{ref} > 10$ | 15.22 | 14.6 |
| 20 – 40 | $6 < M_{ref} \leq 10$ | 11.37 | 10.75 |
| 40 – 100 | $M_{ref} \leq 6$ | 5.65 | 4.75 |

Table 3: Centrality definitions obtained from Glauber calculations using FTPC-E [24].

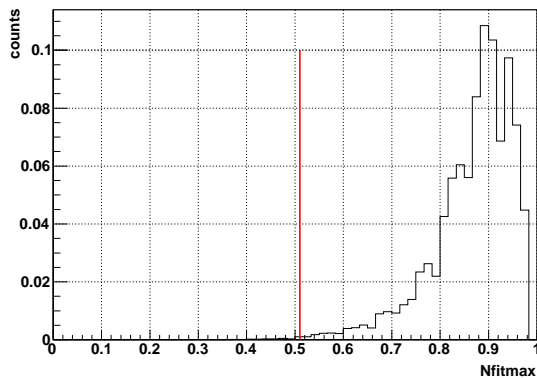
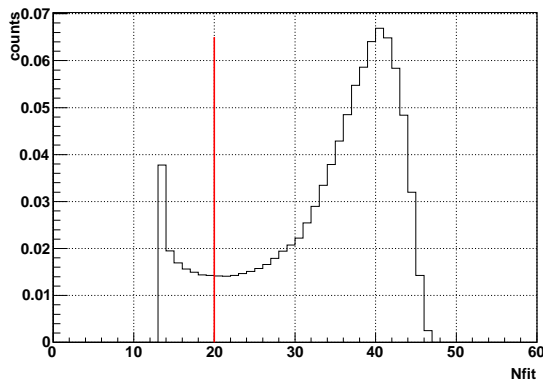


Figure 16: The N_{fitmax} distribution. Red line denotes used cut ($N_{fitmax} > 0.51$).

positrons have typically larger momenta than the background. Hence, the transversal momenta cut was established as $p_T > 1.0 GeV/c$ and in addition momenta cut $p > 1.2 GeV/c$ was used. The second reason for these cuts is a large hadron contamination for low p or p_T electrons and positrons sample. This contamination is apparent in Fig.17 where Bichsel functions for electrons,

pions, protons and kaons are illustrated. All track cuts used in this analysis are listed in Tab.4.

| | |
|--------------|--------------|
| N_{fit} | ≥ 20 |
| N_{fitmax} | > 0.51 |
| $gDCA$ | $< 2cm$ |
| pT | $> 1.0GeV/c$ |
| p | $> 1.2GeV/c$ |

Table 4: The summary of track cuts used in J/ψ analysis in d+Au collisions at $\sqrt{s_N\bar{N}} = 200GeV$.

4.2 Electron identification

In this analysis the J/ψ signal is reconstructed from the electron-positron decay channel. Therefore the main part of the analysis is to identify electrons and positrons. A charged particle is usually identified through the mass-dependent ionization energy loss dE/dx that is measured in the TPC detector. Using the dE/dx information from the TPC, particles with different mass can be distinguished. The distribution of dE/dx for all charged particles as a function of momentum is illustrated in Fig.17.

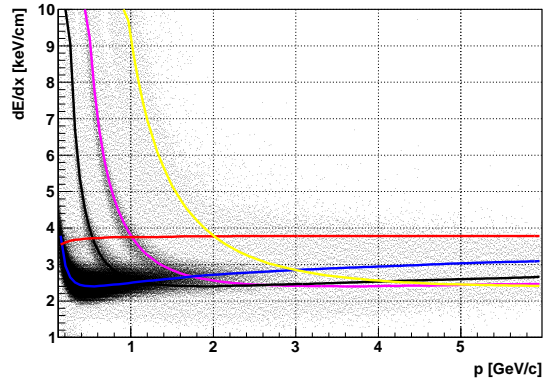


Figure 17: The dE/dx distribution for all charged particles as a function of the track momentum. Bichsel function lines for protons (violet), kaons (black), pions (blue), deuterons(yellow) and electrons (red) are shown.

For distinguish electrons and positrons some cuts based on ionization lost were used. From the electron ionization lost function is clear that electron dE/dx is laying in the range $3 < dE/dx < 5keV/cm$. Due to this and after some purity and efficiency tests the dE/dx cut was established as $3.2 < dE/dx < 4.85keV/cm$. Other quantity related with dE/dx is a nsigma. Its defined as:

$$n\sigma_x = \ln \left(\frac{dE/dx_{measured}}{dE/dx_{BetheBlochx}} \right) / \sigma, \quad (8)$$

where $dE/dx_{measured}$ is a measured ionization lost, $dE/dx_{BetheBlochx}$ is a ionization lost of particle x from BetheBloch function, where x means proton or pion and σ is an error associated with dE/dx measurement and for STAR TPC detector is $\sigma = 0.075$ [25]. These quantity could be calculated for electrons as well but from electron Bischel function is evidently that previous mentioned dE/dx cut is identical. In this analysis were used $n\sigma_{pion}$ and $n\sigma_{proton}$ cuts to obtain the final lepton sample with low hadronic contamination. All these TPC cuts are summarized in Tab.5. The dE/dx distribution after event cuts, track quality cuts and these electron identification cuts are in Fig.18 where Bischel functions for pion, proton, electron, kaon and deuteron are signed by solid lines.

| | |
|----------------------|----------------------|
| $ n\sigma_{proton} $ | > 2.2 |
| $ n\sigma_{pion} $ | > 2.5 |
| dE/dx | $3.2 < dE/dx < 4.85$ |

Table 5: The summary of electron identification cuts used in J/ψ analysis in d+Au collisions at $\sqrt{s_{NN}} = 200GeV$.

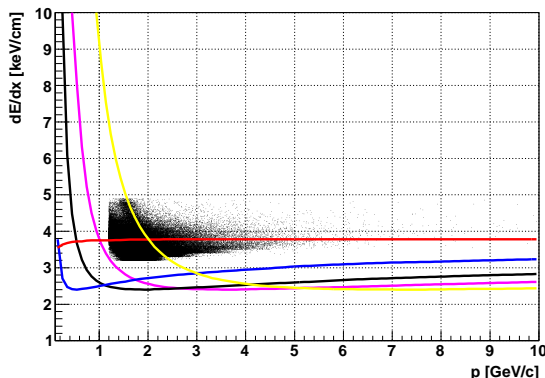


Figure 18: The dE/dx distribution for charged particles that passed TPC cuts as a function of the track momentum. Bischel function lines for protons (violet), kaons (black), pions (blue), deuterons (yellow) and electrons (red) are shown.

An electron could be identified with the TPC and BEMC together that guarantee smaller hadron contamination. Electron candidates are extrapolated to BEMC towers. In the BEMC, particles deposit specific amount of their kinetic energy. Electrons deposit almost all their energy there, while hadrons deposit only its small part. The energy of the corresponding tower is taken to compute the ratio with its corresponding track momentum, p/E . Considering

this fact and the ultra-relativistic state of electrons, p/E must be approximately equal to one. Then the p/E cut ($0 < p/E < 2$) can selected most electrons and reject a large amount of hadrons. Finally, due to the better purity-efficiency ratio only the TPC cuts were used in this analysis.

4.3 The raw J/ψ spectrum

The J/ψ signal in the e^+e^- decay channel is identified as a prominent peak in the dielectron invariant mass spectrum M_{inv} , calculated using the following equation:

$$M_{inv} = 2\sin\frac{\theta}{2}\sqrt{p_+p_-}, \quad (9)$$

where p_+ and p_- are the positron and the electron momenta, respectively, and θ is the open angle between the electron and the positron. Since $M_{J/\psi} = 3.097\text{GeV}$, the estimated peak region is $3.0 < M_{J/\psi} < 3.2$. In every event, many dielectron candidates can be reconstructed. Only some of them are the J/ψ or other decays signal, other combinations are random. These random combinations are called the combinatorial background (N_{bg}). In this analysis the geometric mean N_{bgg} background was calculated. The N_{bgg} is estimated from like-signed pairs (N_{--}, N_{++}) as follows:

$$N_{bgg} = \sqrt{N_{++}N_{--}}. \quad (10)$$

The J/ψ signal is defined as follows:

$$N_{J/\psi} = N_{tot} - N_{bgg}, \quad (11)$$

and the significance of the final J/ψ signal is defined as:

$$sq = \frac{S}{\sqrt{S+2B}}, \quad (12)$$

where S is the J/ψ signal after background subtraction, B is the background and B+S is the total yield of e^+e^- pairs.

Dielectron invariant mass distributions in d+Au at $\sqrt{s_{NN}} = 200\text{GeV}$ collisions before and after background subtraction are shown in Fig.19. The significance of the J/ψ signal and the final signal size for all centrality were estimated at ($sq = 4.9\sigma; S = 58$). The signal was fitted with a gaussian function. The mean and the sigma of the gaussian fit were found to be (3.11; 0.045)GeV. Another way how to fit the J/ψ signal is a fit with a Crystal ball function. In this analysis was preferred fit with gaussian function.

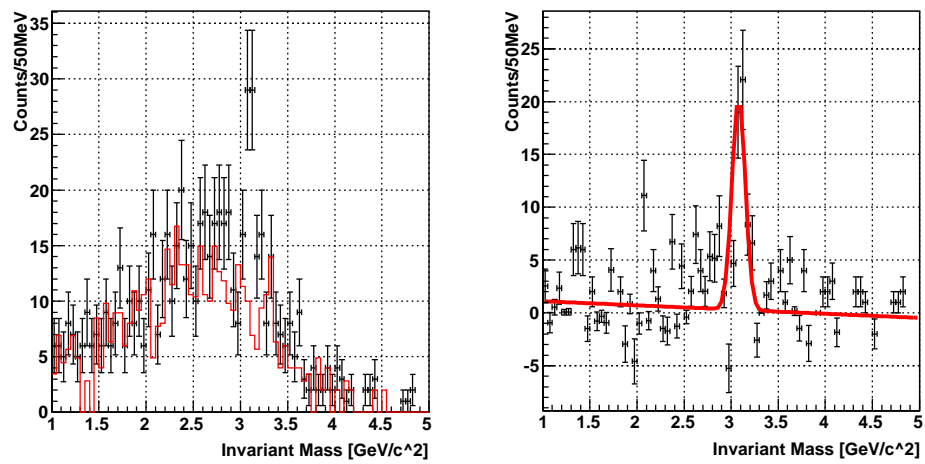


Figure 19: The uncorrected J/ψ invariant mass spectrum before background subtraction on the left and after background subtraction on the right, where red line denotes fitted peak of J/ψ and residual background. Significance is 4.9σ and signal $S=58$. The J/ψ peak is fitted with a gaussian fit with the mean and the sigma found to be (3.11; 0.045)

5 Acceptance and efficiency

5.1 J/ψ reconstruction efficiency

It's clear that not all of J/ψ mesons created in a single collision are reconstructed by this analysis. To obtain the real number of produced J/ψ s, the raw yield of J/ψ s need to be corrected. This difference between real and found number of J/ψ s is due to the detector acceptance, the track reconstruction efficiency and the electron PID efficiency. The J/ψ reconstruction efficiency, included the detector acceptance and the track reconstruction efficiency is determined from reconstruction of Monte Carlo simulated J/ψ s embedded into real events. By this simulation experimental results could be compensated. Simulated J/ψ s were generated with a flat transversal momentum (Fig.20) distribution and they are embedded into real events. Into each event was embedded one simulated J/ψ . It's possible to identify J/ψ and its decay product by their Geant ID.

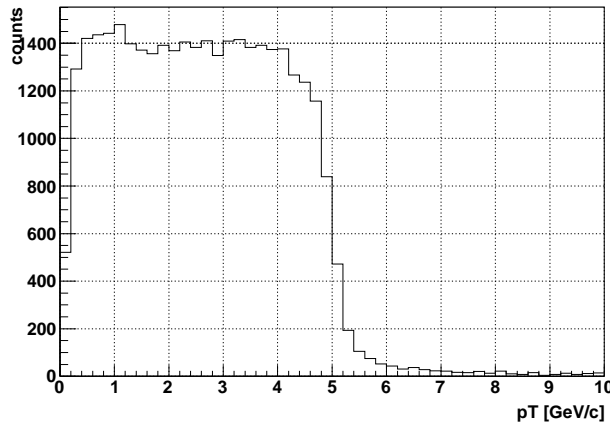


Figure 20: The simulated J/ψ pT distribution before any cut.

Before the estimation of the detector acceptance and the track efficiency the event selection of simulated data was done. Only events with $|Z| < 30cm$ and events which number of tracks matched to the BEMC $N_{BEMC} \geq 1$ were accepted in this analysis, so the same requirement is requested for simulation tracks. The zVertex cut is shown in Fig. 21.

Next it will be discussed the detector acceptance ϵ_{acc} . In this analysis the STAR detector acceptance is evaluated by the pseudo-rapidity cut. Daughter electrons or positrons which pseudo-rapidity η is in the absolute value larger than 1 cannot be reconstructed in the TPC neither their mother J/ψ could be found. The detector acceptance is defined as a fraction of electrons and positrons that complies with pseudo-rapidity cut divided by the total number of electrons and positrons. The detector acceptance estimated for this analysis is shown in Fig. 22.

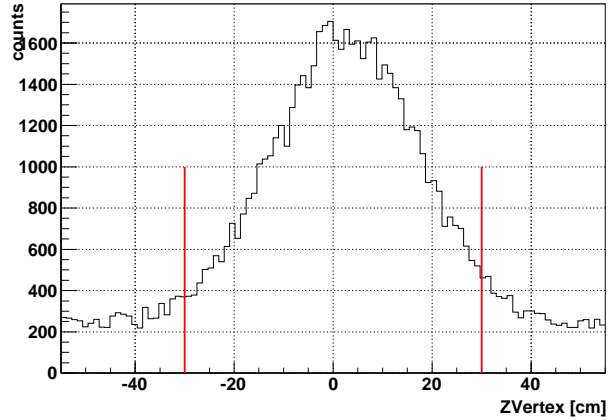


Figure 21: The zVertex distribution, red lines denote the zVertex cut.

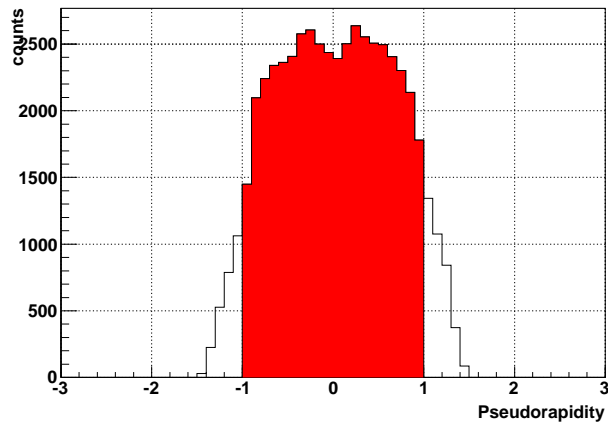


Figure 22: Detector acceptance, the red area represented electrons and positrons that passed η cut.

Then the estimation of the track quality cuts efficiency will be presented. Track cuts, that means all cuts used in this analysis excepted event cuts mentioned before and dE/dx and $n\sigma$ cuts, were applied to embedded tracks to obtain track efficiency correction factor. These cuts are summarized in Table 6.

Single distributions of values used for the track quality estimation N_{fit} , N_{fitmax} and the global DCA with marked cuts are shown in Fig.23, Fig.24 and Fig.25, consequently. The distribution of electrons and positrons momentum and transversal momentum are shown in Fig.27 and Fig.26 consequently.

Reconstructed electrons and positrons from simulated J/ψ s that passed the

| | |
|-------------------|----------------------|
| N_{fit} | ≥ 20 |
| N_{fit}/N_{max} | > 0.51 |
| $gDCA$ | 2 cm |
| pT | $> 1.0\text{ GeV}/c$ |
| p | $> 1.2\text{ GeV}/c$ |

Table 6: The summary of track quality cuts used for the estimation of the track quality cut efficiency.

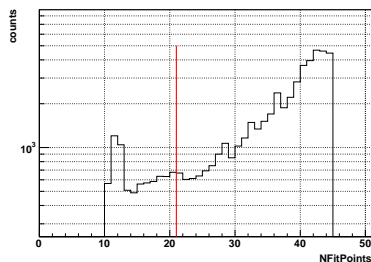


Figure 23: The TPC fit points distribution used to establish the track reconstruction efficiency. The red line denotes the selection cut $N_{fit} > 20$.

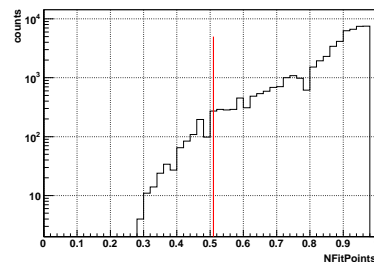


Figure 24: The N_{fitmax} distribution used to establish the track reconstruction efficiency. The red line denotes the selection cut $N_{fitmax} > 0.51$.

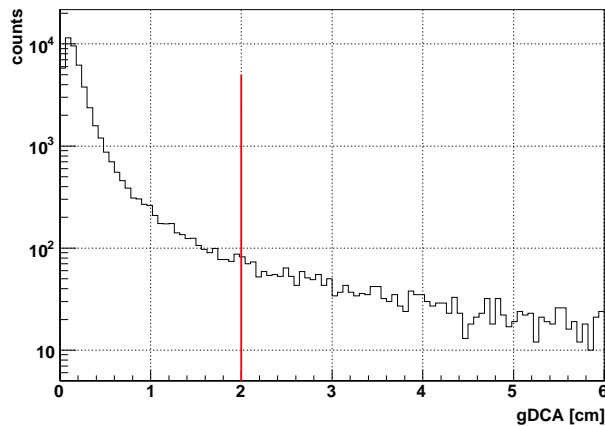


Figure 25: The gDCA distribution, red line denotes gDCA cut ($gDCA < 2$).

track quality cuts were identified and used to reconstruct the original parents, J/ψ mesons. The track reconstruction efficiency is defined as a number of reconstructed J/ψ s that satisfied the quality cuts divided by the total number of

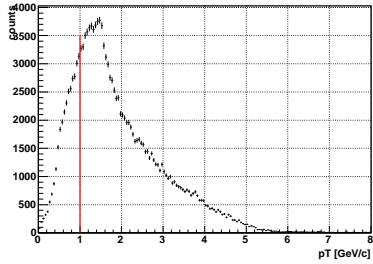


Figure 26: The pT distribution used to establish the track efficiency. The red line denotes the selection cut $pT > 1$ GeV.

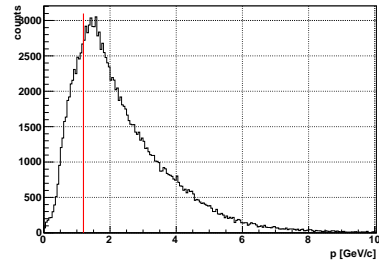


Figure 27: The momentum distribution used to establish the track efficiency. The red line denotes the selection cut $p > 1.2$ GeV.

embedded J/ψ s as a function of transverse momentum. The total J/ψ reconstruction efficiency included detector acceptance, track quality efficiency and event selection efficiency was calculated like a convolution:

$$\epsilon_{rec} = \epsilon_{acc} * \epsilon_{event} * \epsilon_{track}, \quad (13)$$

and it is shown in Fig.28

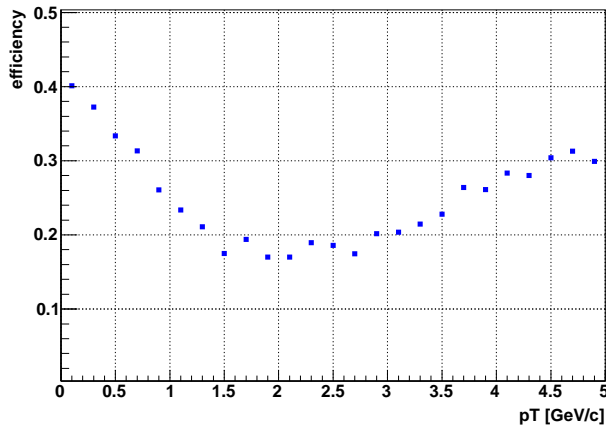


Figure 28: The J/ψ reconstruction efficiency.

5.2 Electron identification efficiency

In this section the electron PID efficiency will be discussed. The electron identification efficiency was defined as a fraction of electrons that passed through event cuts, track quality cuts and also through electron identification cuts and

all electrons produced in the collision that passed track ant event cuts. The total number of electrons reconstructed in the TPC was calculated by performing a multiple Gaussian fit to the dE/dx distribution in different transversal momentum bins (bin width is 0.1 GeV for p_T smaller than 2GeV and 0.2 GeV for larger p_T). In this part of the efficiency calculation were used real data because the estimation of electron PID efficiency from embedded data is problematic. Electron PID cuts used in this analysis are summarized in Table7.

| | |
|----------------------|----------------------|
| $ n\sigma_{proton} $ | > 2.2 |
| $ n\sigma_{pion} $ | > 2.5 |
| dE/dx | $3.2 < dE/dx < 4.85$ |

Table 7: The summary of electron PID cuts used for the estimation of the electron identification efficiency.

The gaussian fit was determined with respect to Bethe-Bloch functions for pion, proton and electron. Examples of Gaussian fit to the dE/dx distribution are shown in Fig.29 and Fig.30 where the blue gaussian function displays the pion production, the violet gaussian displays the proton production and the red one shows the electron production. Solid lines show dE/dx and sigma cuts.

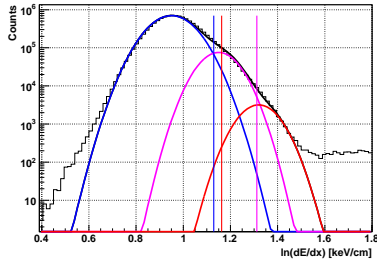


Figure 29: The dE/dx distribution for all charged particles that passed track quality cuts with $1.2 < p_T < 1.3$ GeV/c. Gaussians show pion(blue), proton(violet) and electron(red) yields. The accepted electrons are that on the right from the violet solid line that denotes $n\sigma_{proton}$ cut.

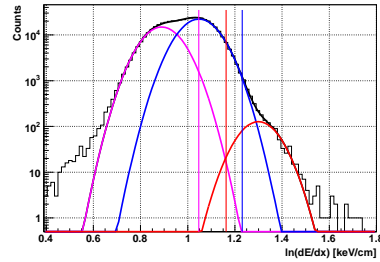


Figure 30: The dE/dx distribution for all charged particles that passed track quality cuts with $2.8 < p_T < 3.0$ GeV/c. Gaussians show pion(blue), proton(violet) and electron(red) yields. The accepted electrons are that on the right from the violet solid line that denotes $n\sigma_{pion}$ cut.

The final electron PID efficiency for single transversal momentum bins are shown in Fig.31.

Total acceptance and efficiency factor is estimated as:

$$\epsilon_{total} = \epsilon_{rec} * \epsilon_{PID1} * \epsilon_{PID2}, \quad (14)$$

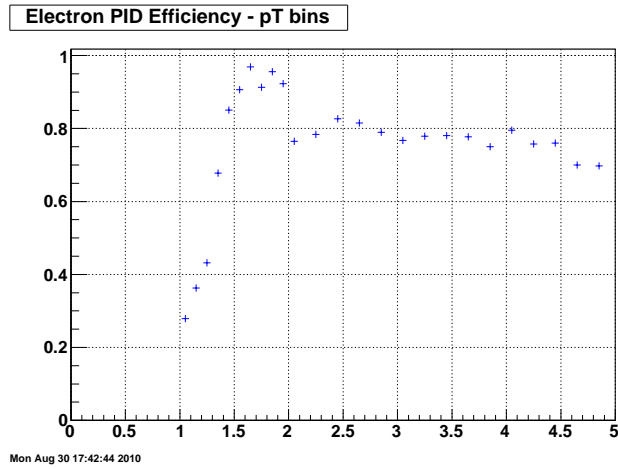


Figure 31: Electron PID efficiency as a function of electron transversal momentum.

where ϵ_{PID1} and ϵ_{PID2} are daughter particles corresponding to mother J/ψ with determined transversal momentum. Finally this factor will be applied to the raw J/ψ pT spectrum. The total efficiency as a function of J/ψ transversal momentum is shown in Fig.32, where red marks denote the total efficiency and blue marks show J/ψ reconstruction efficiency only.

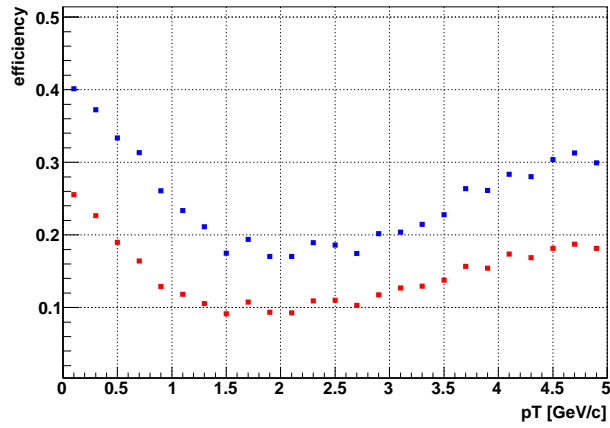


Figure 32: The total efficiency as a function of J/ψ transversal momentum. Blue marks denote J/ψ reconstruction efficiency and red marks denote total efficiency included electron PID efficiency.

6 Corrected J/ψ pT spectrum

In this chapter the corrected J/ψ pT spectrum will be present. For each pT bin of width 1 GeV/c the invariant mass was reconstructed. Only the last bin has a width 2 GeV/c due to the small statistics. Invariant yield was calculated from equation:

$$\frac{\beta_{ee}}{2\pi pT} \frac{d^2N}{dpT dy} = \frac{1}{2\pi pT} \frac{1}{\Delta pT} \frac{1}{\Delta y} \frac{N_{J/\psi}}{N_{event}} \frac{1}{\epsilon_{total}}, \quad (15)$$

where ϵ_{total} is a total efficiency presented in preview chapter, $N_{J/\psi}$ is a number of reconstructed J/ψ s, N_{events} is a total number of collisions, ΔpT is a pT coverage ($\Delta pT = 1$ for 0-1, 1-2 and 2-3 GeV/c bins and $\Delta pT = 2$ for 3-5 GeV/c bin) $\Delta y = 2$. The number of reconstructed J/ψ s, significance and invariant yield for each pT bin is listed in Tab.8.

| pT [Gev/c] | $N_{J/\psi}$ | Significance | Yield |
|------------|--------------|--------------|------------------|
| 0-1 | 29.6 | 2.5 | $4.92 * 10^{-7}$ |
| 1-2 | 28.5 | 2.9 | $3.28 * 10^{-7}$ |
| 2-3 | 18 | 3.5 | $1.13 * 10^{-7}$ |
| 3-5 | 10 | 3.2 | $1.35 * 10^{-8}$ |

Table 8: List of the number of J/ψ s reconstructed in each pT bin, signification and invariant yield.

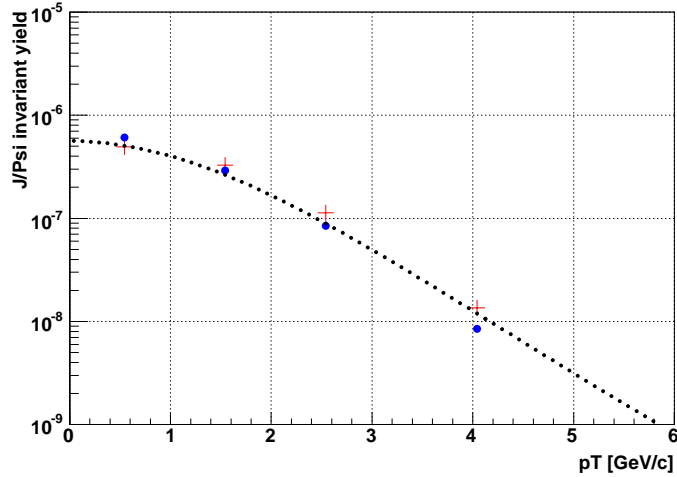


Figure 33: The corrected J/ψ pT spectrum. Red marks show result obtain from this analysis, blue marks show another result obtain at STAR detector[24] and the dotted line is a fit to the PHENIX data.

References

- [1] G. Taku, J/ψ Production in High Energy Heavy Ion Collisions at RHIC, Dissertation thesis (2007)
- [2] S. Oda, Production of Charmonia in Cu+Cu and p+p Collisions at $\sqrt{s}=200$ GeV, Dissertation thesis (2008)
- [3] T. Matsui and H. Satz, Phys. Lett. B 178 416 (1986)
- [4] J.K. Dong, J/ψ Production in d+Au and p+p Collisions at $\sqrt{s}=200$ GeV, Dissertation thesis (2004)
- [5] R. Vogt, Ultrarelativistic heavy-ion collisions (2007)
- [6] J.Wolf et al. (STAR Collaboration), STAR detector overview (2003)
- [7] M. Harisson et al., Nucl. Instr. and Meth. A 499 235 (2003)
- [8] <http://www.star.bnl.gov>
- [9] M. Anderson et al. (STAR Collaboration), The STAR Time Projection Chamber: A Unique Tool for Studying High Multiplicity Events at RHIC(2003) [10] Hans Bichsel (STAR Collaboration), Particle identification at STAR-TPC with ions
- [10] Hans Bichsel (STAR Collaboration), Particle identification at STAR-TPC with ionization measurements(2003)
- [11] M.Beddo et al. (STAR Collaboration), The STAR Barrel Electromagnetic Calorimeter (2002)
- [12] M. Sharma, A Study of Fluctuations in Ultra-Relativistic Heavy Ion Collisions, Dissertation thesis (2008)
- [13] B. Alessandro et al. (NA50 Collaboration), Eur.Phys.J.C39:335-345 (2005),arXiv:hep-ex/0412036v1
- [14] R. Arnaldi et al. (NA60 Collaboration), arXiv:0706.4361v1[nucl-ex](2007)
- [15] E.T. Atomssa (PHENIX Collaboration), arXiv:0805.4562v1 [nucl-ex] (2008)
- [16] R.Arnaldi, Quark Matter (2009)
- [17] D. Kikola (STAR Collaboration), J/ψ production in Au+Au and Cu+Cu collisions at $\sqrt{s} = 200$ GeV at STAR, Quark Matter (2009)
- [18] C. Perkins (STAR Collaboration), J/ψ Production in p+p and d+Au Collisions at $\sqrt{s} = 200$ GeV at STAR, Quark Matter (2009)
- [19] M. Anderson et al. (STAR Collaboration),Nucl.Instrum.Meth.A499:659-678 (2003), arXiv:nucl-ex/0301015v1

- [20] J.E. Gonzalez, J/ψ Production in Au+Au Collisions at $\sqrt{s} = 200\text{GeV}$, Dissertation thesis (2006)
- [21] B.I. Abelev et al. (STAR Collaboration), arXiv:0904.0439v1 (2009)
- [22] D. Tlustý, STAR analysis meeting, MIT (2009)
- [23] Stephen Baumgart (STAR Collaboration), J/ψ production at high transverse momentum in p+p and A+A collisions (2009)
- [24] Christopher Powell (STAR Collaboration), J/ψ Production in d+Au collisions at $s_{nn} = 200\text{GeV}$ at the STAR Experiment (2010)
- [25] Ming Shao et al. (STAR Collaboration), Extensive particle identification with TPC and TOF at the STAR experiment (2006)